

The Mott Transition: Recent Results, More Surprises

GABRIEL KOTLIAR

1 Introduction

The interaction-driven metal-insulator transition has fascinated theorists and experimentalists for many years. This transition is named after Sir Nevill Mott who laid down the foundations of our physical understanding of this phenomenon.¹⁻⁴

A periodic system having an odd number of electrons per unit cell must be an insulator (Mott insulator) when the electron-electron correlations are much larger than the bandwidth. In the limit of weak interactions band theory predicts the system to be metallic, so at some critical ratio of the interactions to the bandwidth a metal-insulator transition, the Mott transition, must occur.

The detailed understanding of this phase transition, the Mott transition problem has been elusive. It constitutes one of the most challenging problems in condensed matter physics because of its non-perturbative nature. The absence of a natural small expansion parameter in the region near the transition makes this problem a test case study of non-perturbative many-body physics.

Mott pointed out that if approaching the metal-to-insulator point, the electronic compressibility vanishes and the screening length diverges; the long-range nature of the Coulomb interactions causes the metal-insulator transition to be of the first-order kind. In a disordered medium, the electronic compressibility is finite at the metal-insulator transition allowing for an interesting second-order metal-insulator point at which the conductivity vanishes but the screening length remains finite.⁵ The order of the transition in a periodic system with *short-range* interactions,⁶ the Mott-Hubbard problem, is still a controversial issue. The solution of this problem is a prerequisite for a detailed understanding of the photoemission spectra of transition metal oxides.

We would therefore like to solve the Hubbard Hamiltonian⁶

$$H = - \sum_{\langle i,j \rangle} (t_{ij} + \mu) c_{i,\sigma}^\dagger c_{j,\sigma} + U \sum_i (n_{i\uparrow} - \frac{1}{2})(n_{i\downarrow} - \frac{1}{2}), \quad (1)$$

the 'bare bones' model displaying a metal-insulator transition with short-range interactions. t_{ij} , the hopping matrix elements, can be on an arbitrary lattice and summation over repeated spin indices is assumed. An accurate numerical solution of this Hamiltonian on a three-dimensional lattice is not within reach of available

computers. Perturbative treatments fail in the most interesting region where U and t are comparable. To make progress we must therefore resort to non-perturbative approximate solutions or to the study of soluble models which contain the physics of the original Hamiltonian. The limit of large spatial coordination, where a typical site has m neighbors, the typical hopping matrix element is scaled as $t_{ij} \sim t/\sqrt{m}$ and m goes to infinity⁷ keeps the kinetic energy and the interactions on the same footing. A powerful technique for solving the Hubbard model exactly in the large lattice coordination limit was suggested in ref. 8. This approach is similar in spirit to the Weiss mean-field theory in classical statistical mechanics, but uses quantum impurity models as single-site 'mean-field Hamiltonians'. For a review of these topics see ref. 9, 10.

This development made possible a thorough investigation of the properties of the Hubbard model in the limit of large dimensions.¹¹⁻¹³ It was pointed out^{12,13} that a Mott transition exists in this limit, and a detailed investigation of this phenomenon has been carried out.^{14-20,21,48}

I will present here a pedagogical summary of what we have learnt so far from this line of investigation. The results are quite surprising. I am sure Sir Nevill Mott will be pleased to see that his ideas are still keeping young theorists busy and continue to inspire the development of new techniques in non-perturbative many-body physics.

2 Early Concepts

To put our results in perspective, we summarize in this section some of the basic concepts which were developed to model the metal-insulator transition.

There are two basic paradigms for understanding the evolution of the one-particle spectral function through the metal-insulator transition. They are associated with the work of Hubbard and Brinkman and Rice. Hubbard introduced the notion of Hubbard bands, describing propagating empty and doubly occupied sites in a half-full lattice. For large interaction U these bands, of width $2D$, are separated by a gap of order $U - 2D$. As U is reduced there is a critical value of the interaction U_c , where the two bands merge.⁶ This is the Hubbard picture of the metal-insulator transition. The resulting metallic state is not a Fermi liquid. A sketch of the evolution of the photoemission and inverse photoemission spectra (i.e. the one-particle spectral function) as a function of U/D is shown in Fig. 1.

Brinkman and Rice,²² building on the work of Gutzwiller,²³ began the treatment of the metal-insulator transition from the metallic phase which they described as a (strongly renormalized) Fermi liquid with a characteristic energy scale, the renormalized Fermi energy ε_F^* . As the interaction strength increases this energy scale decreases and eventually vanishes at a critical value of the interaction U_c . In this framework the metal-insulator transition is driven by the disappearance of the Fermi liquid quasi-particles, the vanishing of the quasi-particle residue $Z \approx U_c - U$ and the divergence of the quasi-particle effective mass $m^* \approx 1/(U_c - U)$. From the point of view of the one-particle spectral function, this framework predicts a well-defined peak at the Fermi level with a width that narrows gradually as the transition is approached. This is shown schematically in Fig. 2.

The high-energy features of the spectral function cannot be described within the Gutzwiller-Brinkman-Rice (GBR) variational approach. The slave boson approach

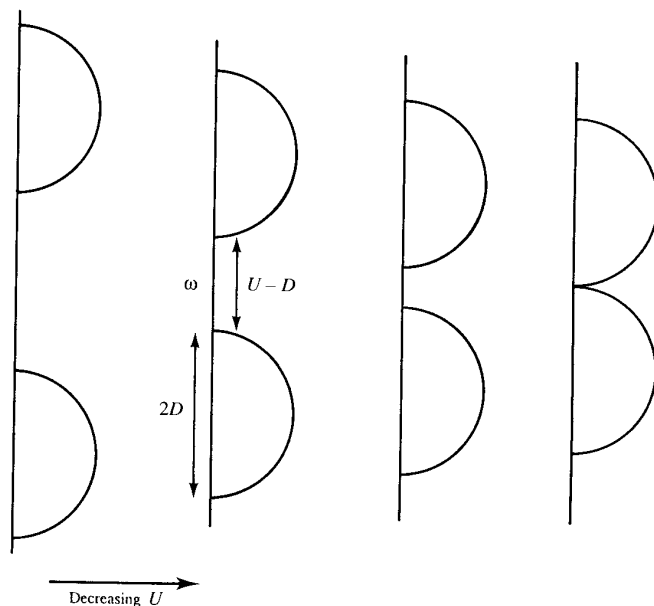


Figure 1 Evolution of the one-particle spectral function at half filling as a function of the interaction in the Hubbard picture. We sketch the imaginary part of the one-particle Green function as a function of frequency for decreasing values of U .

of Kotliar and Ruckenstein²⁵ recovers at low frequency the results of GBR at the saddle point level. Within this slave boson framework, fluctuations around the saddle point can be used to reconstruct the incoherent features of the spectral function.²⁶

In the spirit of the original work of Mott, both of these approaches neglect the incipient magnetic ordering. The magnetism is the consequence rather than the cause of the metal–insulator transition. The opposite point of view was put forward by Slater²⁷ who argued that the metal–insulator transition is always accompanied by long-range antiferromagnetic order, and viewed the doubling of the unit cell which makes the band structure of the system that of a band insulator, as the driving force behind the metal–insulator transition.

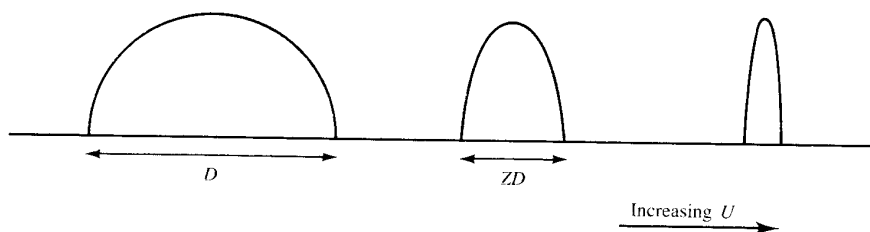


Figure 2 Evolution of the one-particle spectral function as a function of the interaction in the Brinkman–Rice picture. We sketch the imaginary part of the one-particle Green function as a function of frequency for increasing values of U .



Metal-Insulator Transitions Revisited

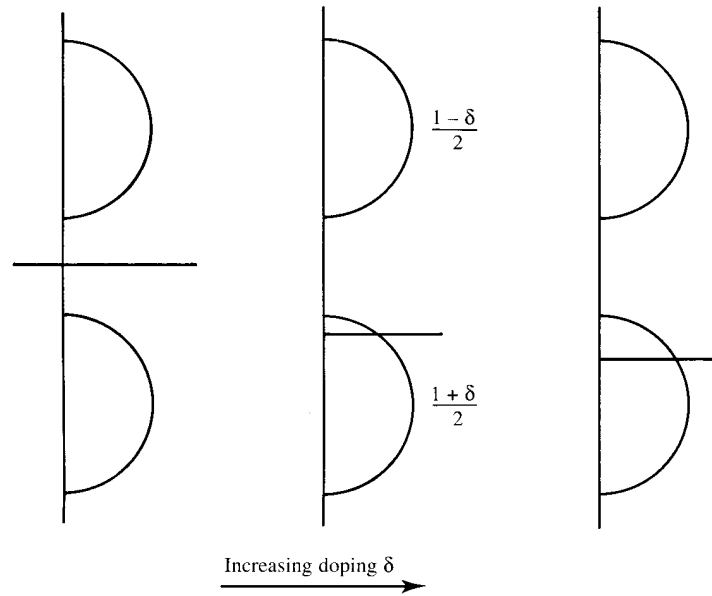


Figure 3 Evolution of the spectral function upon doping in the Hubbard (rigid band) picture. We sketch the imaginary part of the one-particle Green function as a function of frequency for increasing values of doping. The horizontal line indicates the position of the Fermi level.

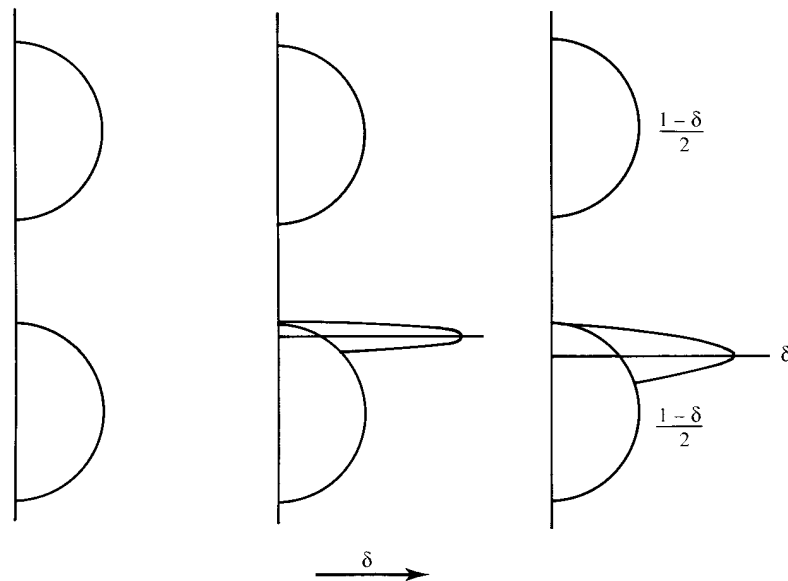


Figure 4 Evolution of the spectral function upon doping in the slave boson approach. We sketch the imaginary part of the one-particle Green function as a function of frequency for increasing values of doping δ . The horizontal line indicates the position of the Fermi level.

A closely related question is the evolution of the spectral function as one dopes the Mott insulating state. In the Hubbard picture, no new states are generated upon doping. Upon doping the chemical potential moves into the Hubbard band, and the spectral weights in the one-particle spectral function change as indicated in Fig. 3. This is called the rigid band picture because the nature of the states that contribute to the spectral function of the doped insulator are the same as those in the insulating state. Only the matrix elements (weights) for adding and removing a particle change.²⁴

This picture should be contrasted with the picture which emerged from slave boson calculations.²⁶ Here, upon doping, new states, which are qualitatively different from those pre-existing in the insulator are generated when a finite concentration of holes is introduced into the Mott insulator. The Hubbard bands in the large- U limit carry weight $(1 - \delta)/2$, while the new states which are similar in nature to multiparticle Kondo resonances carry weight δ . This is shown schematically in Fig. 4. Explicit calculations using the slave boson scheme proposed by Kotliar and Ruckenstein show that the position of the resonances for infinitesimal electron (hole) doping is the bottom (top) of the upper (lower) Hubbard band respectively.²⁶

We will show in the next section how our recent mean-field approach to the Mott transition has allowed us to reconcile these, at first sight, conflicting points of view, in the framework of an internally consistent approximation which is exact in a well-defined limit, that of infinite dimensionality. Furthermore this framework allowed us to make quantitative calculations that can be compared with experimental findings on various transition metal oxide compounds.

3 Model and Methodology

To clarify the physical origin of the Mott transition and its interplay with magnetism it is essential to study lattices which have magnetic frustration, i.e. in the localized phase the spin degrees of freedom interact with magnetic exchange constants of different signs. To be definite we will describe the results for a Bethe lattice with coordination m , with hopping matrix elements between nearest neighbors given by t_1/m and next-nearest neighbor t_2/m^2 in the limit that the coordination number m goes to infinity. This lattice for $m = 3$ is schematically depicted in Fig. 5. In the non-interacting limit the local density of states is a semicircle

$$\rho(\varepsilon) = \frac{2}{\pi D} \sqrt{1 - \left(\frac{\varepsilon}{D}\right)^2} \quad (2)$$

with a half bandwidth $D = 2t$ and $t = (t_2^2 + t_1^2)^{1/2}$.

When $t_2 = 0$ our model reduces to the ordinary Bethe lattice, which is bipartite and unfrustrated, so t_2/t_1 measures the degree of magnetic frustration. We refer to the case $t_2 = t_1$ as the fully frustrated model because one can realize the equations in this case on a fully connected graph, with random hopping matrix elements.¹²

We point out, however, that the results that will be described below are a qualitative guide to the behavior of more general frustrated lattices, such as the hypercubic lattice with nearest- and next-to-nearest-neighbor hopping matrix elements.

The essential idea of the mean-field approach is to replace the quantum many-body problem by a single-site quantum problem, an impurity model in an effective medium which is solved for self-consistency.⁹

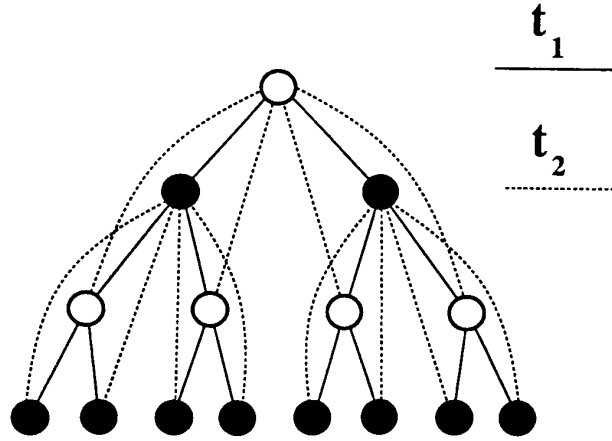


Figure 5 Bethe lattice with nearest and next-nearest hopping matrix elements as a realization of the two-sublattice frustrated model from the work of Rozenberg *et al.*

For the Hubbard model in the paramagnetic phase the associated impurity model is an Anderson model defined by the effective action

$$S_{\text{eff}}[c, c^\dagger] = \sum_{\sigma} \int d\tau d\tau' c_{\sigma}^{\dagger}(\tau) G_0^{-1}(\tau - \tau') c_{\sigma}(\tau') + U \int_0^{\beta} d\tau [n_{i\uparrow}(\tau) - \frac{1}{2}][n_{i\downarrow}(\tau) - \frac{1}{2}]. \quad (3)$$

The propagator G_0 plays the role of a Weiss field and, restricting to the paramagnetic phase, obeys the self-consistency condition

$$G_0^{-1}(i\omega_n) = i\omega_n + \mu - t^2 G(i\omega_n) \{G_0\} \quad (4)$$

where $G(i\omega_n) = -\int_0^{\beta} \exp(i\omega_n \tau) \langle T_{\tau} c(\tau) c^{\dagger}(0) \rangle_{S_{\text{eff}}[G_0]}$ is a functional of $G_0(i\omega_n)$. After self-consistency is attained, one can evaluate this functional at the self-consistent value of the Weiss field function and then it gives the local Green function $G(i\omega_n)$ of the Hubbard model.

The mean-field approach can also be used to investigate the occurrence of magnetic long-range order.⁹ In the Néel state with magnetic sublattices A and B the local Green functions and the Weiss fields are spin and sublattice dependent, $G_{A\sigma} = G_{B-\sigma}$. This results in a different self-consistency condition. In the Bethe lattice, a magnetically unfrustrated lattice, we have

$$G_{0A\sigma}^{-1} = i\omega + \mu - t^2 G_{B\sigma} \quad (5)$$

$$G_{0B\sigma}^{-1} = i\omega + \mu - t^2 G_{A\sigma} \quad (6)$$

where A denotes one sublattice and B the other. The two impurity Green functions G_A and G_B are evaluated independently given $G_{0A\sigma}$, $G_{0B\sigma}$ and the single-site action S defined above.

The mean-field equations are coupled functional equations to be solved for the Weiss field G_0 and the local Green function.⁹ The mean-field equations in the ordered phase depend on the lattice under consideration. It is instructive to study

lattices where the magnetism is frustrated. For this purpose we introduced the two-sublattice fully frustrated model.¹⁶ In this case the mean-field equations are given by

$$G_{0A\sigma}^{-1} = i\omega + \mu - t_1^2 G_{A\sigma} - t_2^2 G_{B\sigma} \quad (7)$$

$$G_{0B\sigma}^{-1} = i\omega + \mu - t_1^2 G_{B\sigma} - t_2^2 G_{A\sigma}. \quad (8)$$

t_1/t_2 is a measure of the degree of frustration. A lattice which realizes this model is a Bethe lattice with nearest neighbor and next-nearest-neighbor hops shown in Fig. 5. Another realization is in a two-sublattice fully connected random model.¹⁶

The power of our model,⁸ as compared with earlier attempts to attack the many-body problem in large dimensions,²⁸⁻³¹ resides in the existence of a large body of knowledge on quantum impurity models. We have relied on this knowledge to develop good numerical algorithms and analytic approximations to solve the mean-field equations. The essential insight is to use *reliable* approximations to calculate $G\{G_0\}$ in Eq. (4). This calculation is done using the effective action of Eq. (3); this step captures the local aspects of the problem. The self-consistency condition (4) then brings back the lattice aspect.

We have used several techniques for the analysis of the mean-field equations. They range from qualitative arguments and analytic perturbative schemes to numerical methods based on quantum Monte Carlo (QMC),^{11,13} exact diagonalization (ED),^{17,32} and second-order perturbative calculations (2OPT).^{14-16,33} To obtain details of the low-energy behavior we have developed the projective self-consistent method which is the lattice equivalent for large- d problems of the Wilson renormalization group method.¹⁹ The physical picture that I will describe below has been confirmed and cross-checked by all these methods. Throughout the chapter, we take the half bandwidth $D = 2t = 1$.

Notice that the mean-field Eq. (4) can be derived from the free-energy functional^{9,41}

$$F[G(i\omega_n)] = \sum_n \frac{t^2}{2} G(i\omega_n)^2 - \log Z_{AM} [\Delta(i\omega_n) = t^2 G] \quad (9)$$

of the local Green function, $G(i\omega_n)$. Z_{AM} in Eq. (9) is the partition function of an Anderson impurity model with its hybridization function $\Delta(i\omega_n) = \sum_k V_k^2 / (i\omega_n - \epsilon_k)$ set equal to $t^2 G(i\omega_n)$. The Baym-Kadanoff construction can be used to show that at the saddle point (9) gives the free energy of this system. This free energy, and its generalization to the antiferromagnetic phase, can be used to calculate the phase diagram.

Notice that only at zero temperature is there a sharp difference between a metal and an insulator. The spectral function at zero frequency of an insulator (i.e. the one-particle density of states) is zero. On the other hand a metal has a non-zero density of states for adding or removing a particle. The one-particle density of states at the chemical potential

$$\rho = \frac{1}{i\pi} \lim_{\omega_n \rightarrow 0^-} G(i\omega_n) \quad (10)$$

plays the role of a Landau order parameter for the metal-insulator transition in a clean system. It is very close in spirit to the Wegner order parameter for the localization problem in its non-linear sigma model formulation.⁴³ When the system is insulating, it is sensitive to spatial and temporal boundary conditions, and the retarded and advanced Green functions have the same limit as the frequency is set to

zero. When the system is metallic, the advanced and the retarded Green functions tend to different limits as the frequency goes to zero. This difference is a branch cut discontinuity in the one-particle Green function in Eq. (10), which therefore can be used as an order parameter in the metallic phase.

In the mean-field approach that we have developed, the local Green function plays the role of an order parameter *function*.⁸ We expect that not only the zero-frequency limit of this function, but also the characteristic width at low energies, will be important for the mean-field description of a Mott–Anderson transition in an interacting disordered system.⁴¹

4 Phase Diagram

An important issue is the qualitative structure of the phase diagram of the model – the phase diagram of V_2O_3 .^{39,40,42} It displays a remarkable first-order transition between a paramagnetic metal to a paramagnetic insulating phase at finite temperature in addition to a phase transition into an antiferromagnetic insulating phase which occurs at lower temperatures. One would like to know whether the Hubbard model by itself can produce such a rich phase diagram, or if it is necessary to consider more complicated Hamiltonians describing the electron–phonon interactions and the structure and chemistry of this compound more explicitly.

This issue has been debated extensively in the literature but given the nature of the approximate solutions it has not been settled. It is argued on the basis of functional integral methods^{34–37} that the phase diagram of the Hubbard model on the three-dimensional hypercubic lattice displays a finite temperature first-order metal–insulator transition in addition to the Néel transition line. This is not observed in Monte Carlo calculations,³⁸ which show a second-order phase transition between a paramagnetic and an antiferromagnetic phase.

We have settled this long-standing issue within the limit of large lattice coordination.¹⁶ The phase diagram in the unfrustrated case is identical to that found in Monte Carlo calculations.^{11,15,16} There is a second-order transition between a paramagnetic phase and a low-temperature Néel state. The phase diagram of the Hubbard model on the Bethe lattice is shown in Fig. 6. In this case one can understand the insulating phase by continuing the Slater insulator from the small- U to the large- U regime.

As the degree of frustration is increased the Néel temperature is reduced. In particular for intermediate values of the frustration, i.e. when the hopping parameters in our model take the value $t_1^2 = 0.75t^2$, $t_2^2 = 0.25t^2$, the Néel temperature is well below a line of first-order transitions ending in a second-order critical point. The first-order metal–insulator transition becomes physically relevant, realizing Mott’s scenario. The phase diagram of the Hubbard model with intermediate frustration is shown in Fig. 7.

A line of first-order transitions separates the paramagnetic metal from the paramagnetic insulating phase. At higher temperatures, one can go continuously between these two phases, through two sharp crossover regions. One crossover region is associated with the disappearance of the Kondo resonance and takes place when the temperature is comparable with the renormalized Fermi energy. This is a continuation of the first-order line, which above the second-order point turns into a crossover line. The second crossover is between a semiconducting regime where the temperature is comparable with the gap of the insulator and an insulating regime

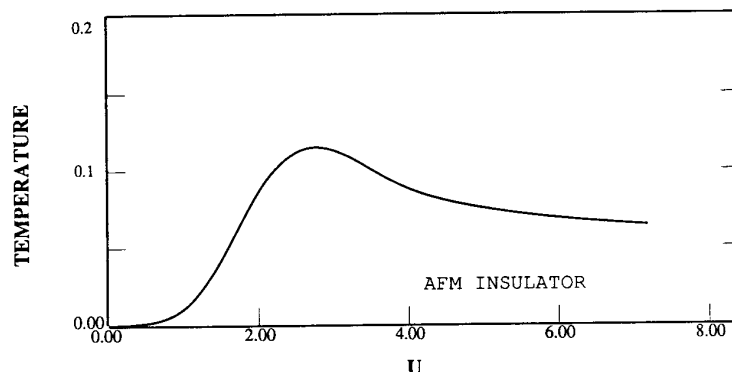


Figure 6 Phase diagram of the half-filled Hubbard model on the (unfrustrated) Bethe lattice with infinite coordination, from the work of Rozenberg *et al.*

where the gap is much larger than the temperature. This crossover is indicated by the shaded region in Fig. 7 and occurs when the temperature is comparable with the insulating gap. At lower temperatures antiferromagnetic order sets in. There is also a narrow region of metallic antiferromagnetism (AFM). This phase diagram is very similar to that of V_2O_3 where the transition is driven by varying pressure, temperature, and composition. U_{AF1} and U_{AF2} are the critical values for the onset of metallic and insulating antiferromagnetism respectively.

The nature of this metal-insulator transition is clarified by studying the fully frustrated limit $t_1 = t_2$, which does not Néel-order at any finite temperature. Our results for the fully frustrated Hubbard model at half filling are summarized in the schematic phase diagram shown in Fig. 8.

There is a region of parameter space where the mean-field equations have two different solutions: one metallic and the other insulating. The metallic solution is

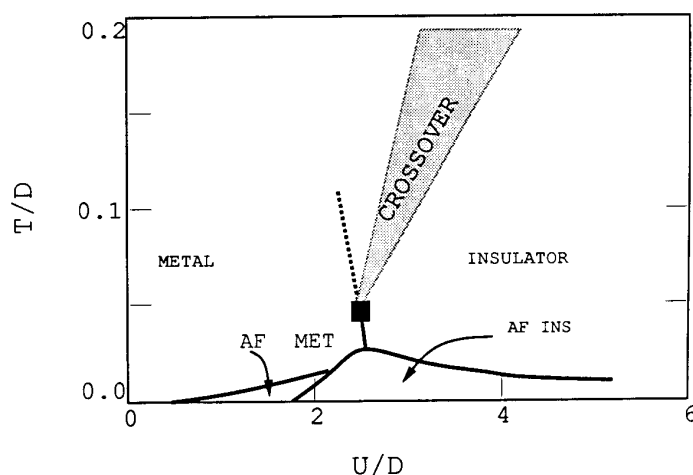


Figure 7 Phase diagram of the Hubbard model with intermediate values of the magnetic frustration $t_1^2 = 0.75t^2$, $t_2^2 = 0.25t^2$ from the work of Rozenberg *et al.*

Metal-Insulator Transitions Revisited

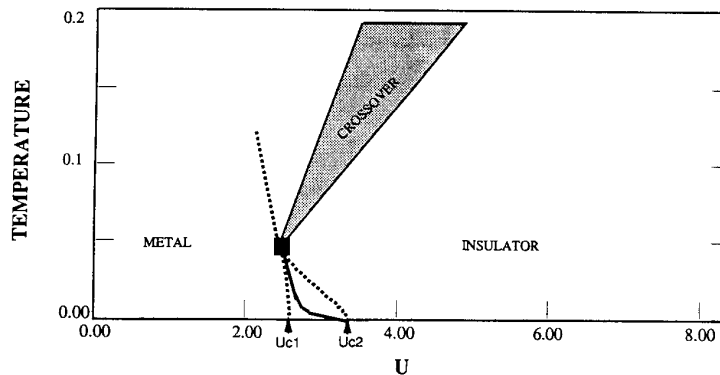


Figure 8 Phase diagram of the fully frustrated model. It displays a line (solid line) of first-order phase transitions and the region where two solutions coexist (region bounded by the two dotted lines). At higher temperatures there is a crossover region (shaded area) between a metallic-like and an insulating-like regime.

found to break down along the dotted line ending at zero temperature at U_{c2} , and the insulating one at the dotted line ending at zero temperature at U_{c1} . The locus of the points where the free energies of the two solutions cross defines a first-order line where several quantities experience a jump. This line ends in a second-order point at $T \approx 0.05$. At higher temperatures there are two crossover regions as discussed earlier. At $T = 0$, we have shown¹⁷ using the exact diagonalization method that the metallic state is lower in energy; therefore the first-order line ends in a $T = 0$ second-order critical point as the critical value (denoted U_{c2} in the figure) is approached. The ED and the QMC method confirmed that the phase diagram obtained from 2OPT, which is shown in Fig. 8, is qualitatively correct. The ED method gives $U_{c1} \approx 2.4$ and $U_{c2} \approx 2.9$. For comparison we point out that the Hubbard approximation, which uses the $t = 0$ limit as a starting point, gives $U_c \approx 1.75$, and the Brinkman-Rice approach, which starts from the $U = 0$ limit, gives $U_c \approx 3.3$.

At zero temperature, in the coexistence region shown in Fig. 8 the metallic and the insulating states are metastable states of the Landau-Ginzburg functional.

At finite temperatures there is no qualitative difference between a metal and an insulator because both have a finite spectral function at low frequencies. As a result the metal-insulator transition at finite temperatures is of the first order. The spectral function across the first-order boundary in Fig. 8 in section jumps from a large value on the metallic side to a small value on the insulating side. The metal-insulator transition at finite temperatures is very similar to the liquid-gas transition. The first-order line ends in a second-order critical point. One can go continuously from the metal to the insulating phase in the phase diagram in Fig. 8 by raising the temperature.

5 Evolution of the Spectral Function Near the Mott Transition at Half Filling

Zhang, Rozenberg and Kotliar (ZRK) studied the evolution of the spectral function at zero temperature. Based on 2OPT and the assumption that the metallic solution was the lowest in energy at zero temperature they concluded that the metal-

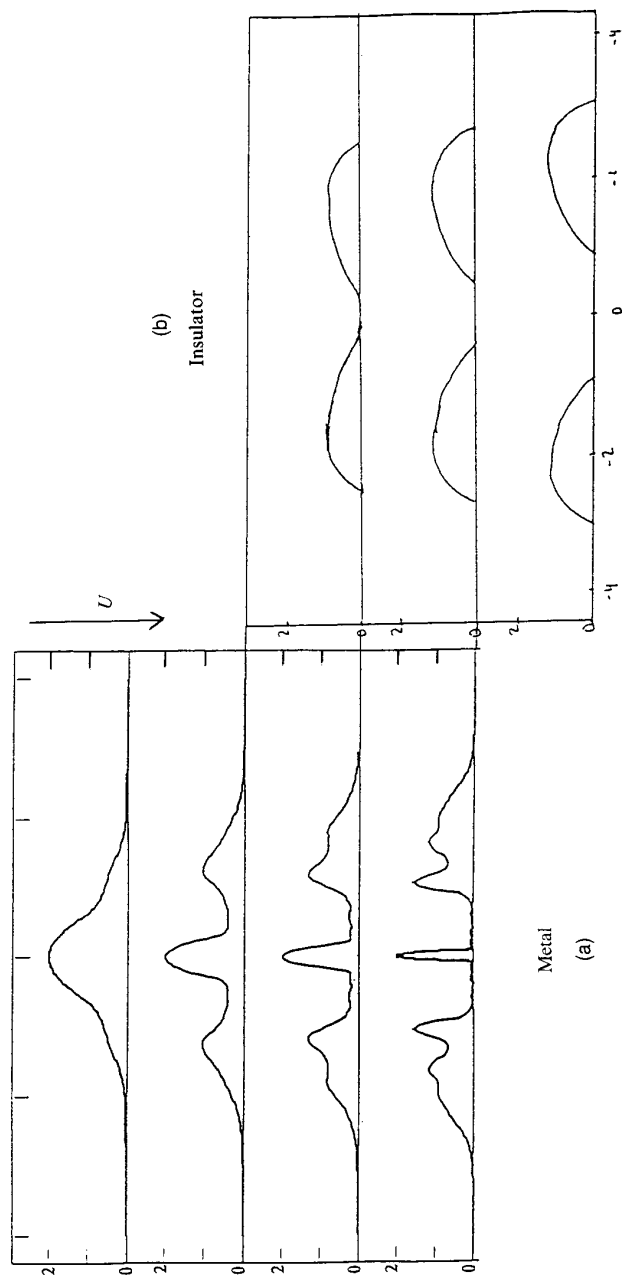


Figure 9 A qualitative sketch of the evolution of the zero-temperature spectral function according to ZBK. (a) A metallic solution (b) the insulating solution. Notice the region of coexistence of metallic and insulating solutions.

insulator transition at U_{c2} was *continuous*. The metal–insulator transition is driven by the divergence of the effective mass as in the Brinkman–Rice scenario. They observed the surprising fact that at U_{c2} the Mott–Hubbard gap was finite (non-zero) and well formed at the transition. Earlier work using slave bosons²⁶ had predicted that the collapse of the low-energy resonance would coincide with the closure of the Mott–Hubbard gap.

The metallic solution for intermediate values of U is characterized by a narrow quasi-particle peak at the Fermi energy with a width e_F^* that goes to zero as $U_{c2} - U$, plus two relatively well-defined high-energy incoherent features at $\pm U/2$. This picture of the spectral function is very natural from the point of view of the mean-field theory, which represents the metal as an Anderson impurity model.⁸ The evolution of the spectral function according to ZRK is sketched in Fig. 9a.

Later work^{16,17,19} demonstrated that the assumptions and qualitative features of the scenario proposed by ZRK were completely correct in the exact solution of the large- d Hubbard model, and that the 2OPT qualitative predictions for many physical quantities were quite accurate.

Since the gap at U_{c2} is finite the insulating solution can be continued below U_{c2} . This is shown in Fig. 9(b). An important observation¹⁶ is that the gap in the insulator is smaller than the distance between the upper and lower Hubbard band-like features that exist in the metallic solution.

While the insulating solution at zero temperature has higher energy than the metallic solution in the fully frustrated model, this energy difference is very small. Finite frustration does stabilize the antiferromagnetic state at a low energy as shown in Fig. 7. The paramagnetic insulator solution then acquires physical relevance since when the frustration is large but not infinite, the antiferromagnetic state that results has a spectral function which is rather close to the paramagnetic insulating one. In the partially frustrated case there is a narrow window of the parameter U which results in a metallic antiferromagnetic state at zero temperature. Above the Néel temperature, in this regime of interactions, the Slater gap is destroyed and the spectral function resembles the metallic solution of the fully frustrated model at zero temperature.

The determination of the critical behavior near the zero-temperature metal–insulator transition point is the subject of various publications.^{12,14,19} The quasi-particle residue as function of U is sketched in Fig. 10.

Near the transition $U_c = U_{c2} = 2.9$ ¹⁹

$$\frac{m^*}{m} = Z^{-1} \approx 0.91 \left[1 - \left(\frac{U}{U_c} \right) \right]^{-1}. \quad (11)$$

For comparison it is worthwhile to notice that in the Gutzwiller approximation the critical value of the interaction is $U_{BR} = 3.37$ and this value is very close to the value obtained in second-order perturbation theory. The double occupancy $Doub \equiv n_\uparrow n_\downarrow$, as a function of U , also exhibits critical behavior:

$$\langle Doub \rangle = 0.235 \left(\frac{U_c - U}{U_c} \right) + 0.015. \quad (12)$$

The Brinkman–Rice approach predicts the critical vanishing of the doubly occupancy at the transition $\langle Doub \rangle_{BR} \approx 0.07(U_{BR} - U)$, but misses the additive non-singular part. Since the double occupancy measured in the insulating solution also

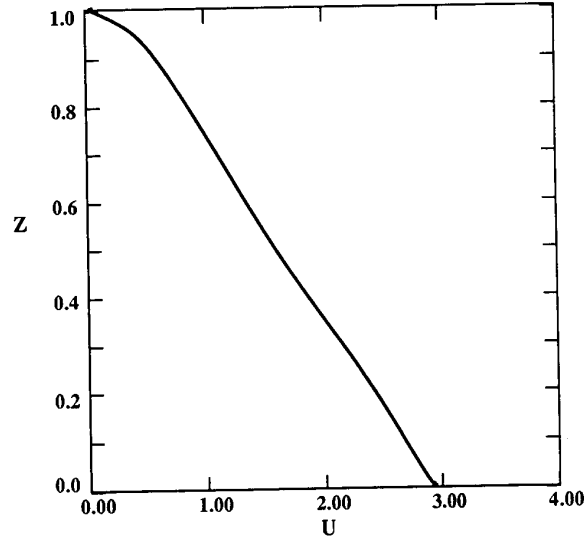


Figure 10 The quasi-particle weight of the half-full Hubbard model Z as a function of the interaction U .

contains a singular part, it is interesting to subtract them. The result

$$\langle Doub \rangle_M - \langle Doub \rangle_I \approx 0.05(U_c - U) \quad (13)$$

is close to the Brinkman–Rice answer. From (13) we can calculate the energy difference between the coexistent metallic and the insulating solutions at zero temperature:

$$E_M - E_I = \int_{U_c}^U dU \langle Doub \rangle_M - \langle Doub \rangle_I \approx -0.025(U - U_c)^2. \quad (14)$$

The inverse magnetic susceptibility χ_s^{-1} in units of $g\mu_B/2$ is a sum of a critical and a noncritical part near the transition. The results of numerical calculations for intermediate values of U/D can be parametrized as¹⁶

$$\chi^{-1} \approx 0.7 \left(1 - \frac{U}{U_c} \right) + J. \quad (15)$$

In the insulator phase $\chi^{-1} \approx (J + T)$. The magnetic susceptibility remains finite at the transition owing to the existence of a non-zero superexchange constant $J = 2t^2/U = D^2/2U$. The Wilson ratio as a function of the interaction U is shown in Fig. 11.^{16,18} It is approximately unity for $U/D < 2$ and is found to vanish as one approaches the critical point since, while the specific heat diverges as $1/Z$, the magnetic susceptibility is cut off by $\min \{T^{-1}, J^{-1} = 2U/D^2\}$. This is an artefact of the infinite-dimensional limit, which keeps the exchange interaction between two spins in neighboring sites of order $1/d$. We would expect the magnetic superexchange to cut off the divergence in the specific heat as in the large- N solution of the t - J model in ref. 44.

This should be contrasted with the behavior of the local spin susceptibility, $\chi_{loc} = \sum_q \chi(q)$, which diverges approaching the Mott transition. This led us¹⁹ to

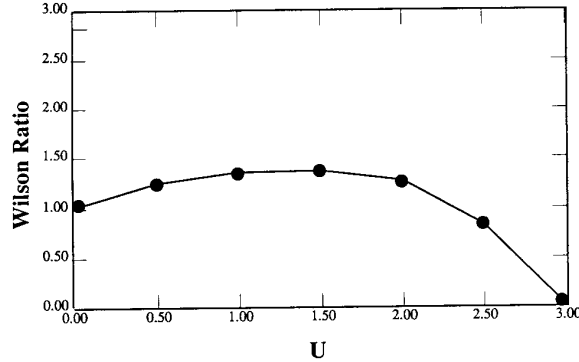


Figure 11 Wilson ratio as function of the interaction U .

define a generalized Wilson ratio, R_g , defined as the ratio of χ_{loc}/γ to its non-interacting ($U = 0$) value, $\chi_{\text{loc}0}/\gamma_0$. R_g measures the enhancement of the susceptibility at a generic q on the Brillouin zone. The different behavior of the susceptibility at different values of q can be understood by sketching a caricature of χ in a large but finite number of dimensions along a symmetry line. It has two non-generic values at the origin and the corner of the Brillouin zone, separated from the generic value by a boundary layer that shrinks as the dimensionality tends to infinity. The behavior of χ_{loc} was analysed in ref. 19. After expressing the vanishing of the weight in the central peak of Fig. 9 as $w \approx 5.5(U_c - U)$, we obtained

$$\chi_{\text{loc}}^{-1} \approx 0.7(U_c - U), \quad R_g \approx 2.8. \quad (16)$$

It is also interesting to study the behavior of the lifetime as obtained from the imaginary part of the retarded self-energy. It is quadratic in frequency and has a stronger divergence as $U \leftarrow U_c$ than the quasi-particle residue. Defining a renormalized energy scale $\Delta \approx wD$ which vanishes as U approaches U_c we express

$$\text{Im } \Sigma(\omega + i0^+, T) = -\frac{1.1}{\Delta^2} \frac{\omega^2 + \pi T^2}{D}. \quad (17)$$

A related quantity is the low-temperature resistivity. In mean-field theory, we write

$$\rho(T) = \left(\frac{\omega_{p0}}{2\pi}\right)^{-2} 2 \text{Im } \Sigma(T) = AT^2 \quad (18)$$

where the plasma frequency of the non-interacting system is defined by $(\omega_{p0}/2\pi)^2 = (e^2/\hbar a)2 \sum_{\mathbf{k}} v_{kx}^2 \delta(\varepsilon_{\mathbf{k}})$. Using $1/(e^2/\hbar) \approx 4 \text{ K}\Omega$ and a typical distance in the cubic perovskite structure of 8 \AA , we find the ratio $A/\gamma^2 \approx 13 \mu\Omega \text{ cm K}^2 \text{ mJ}^{-2}$. This is the order of magnitude found in heavy fermion systems but is much bigger than in ordinary transition metals like Pd or Ni where this ratio is one order of magnitude smaller, i.e. $0.4 \mu\Omega \text{ cm K}^2 \text{ mJ}^{-2}$.⁴⁵

The imaginary part of the dynamical spin susceptibility is linear in frequency and diverges as the specific heat squared:

$$\lim_{\omega \rightarrow 0} \frac{\chi_s''(\omega + i0^+)}{\omega} = 36/(D\omega)^2 \quad (19)$$

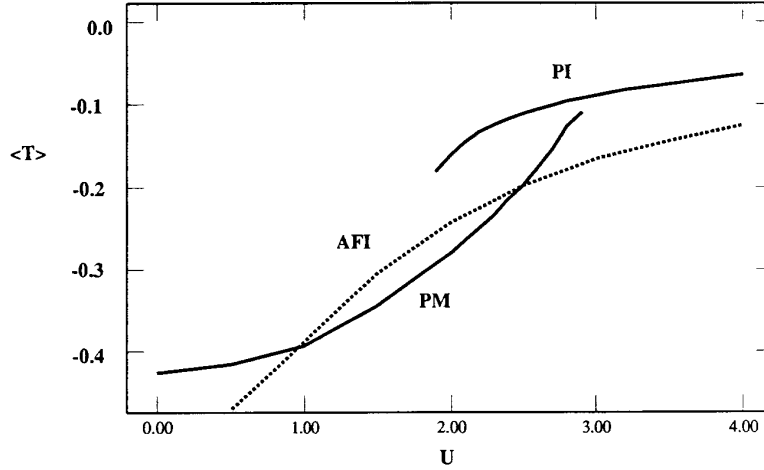


Figure 12 Kinetic energy in the paramagnetic (metal and insulator) and in the unfrustrated antiferromagnetic insulating phase as a function of the interaction U .

Combining this equation with (15) not too close to the transition, so that we can neglect the exchange constant J , we can estimate a Korringa product:

$$\lim_{\omega \rightarrow 0} \frac{\chi_s''(\omega + i0^+)}{\omega(\pi/2)\chi^2} \approx 2.7. \quad (20)$$

The charge compressibility, on the other hand, is found to vanish at the metal-insulator transition:

$$\frac{dn}{d\mu} \approx \frac{0.5}{D} \left(1 - \frac{U}{U_c}\right). \quad (21)$$

The critical parts of the charge and spin susceptibility in expressions (21) and (15) are close to the predictions of the Brinkman-Rice treatment.

The optical conductivity of the model at $T = 0$ can be expressed as

$$\sigma(\omega) = \frac{\omega_p^{*2}}{4\pi} \delta(\omega) + \sigma_{\text{reg}}(\omega) \quad (22)$$

where the coefficient in front of the delta function is the Drude weight and ω_p^* is the renormalized plasma frequency. In the presence of disorder $\delta(\omega)$ is replaced by a Lorentzian of width Γ .

The total kinetic energy is related to the conductivity by the f sum rule

$$\int_0^\infty \sigma(\omega) d\omega = -\frac{\pi e^2 \langle T \rangle}{2\hbar^2 a} = \frac{\omega_p^2}{4\pi} \quad (23)$$

where e is the electron charge and a the lattice constant.

The expression above is valid in any dimension; the sum rule contains contributions from a Drude part at zero frequency and an incoherent part at finite frequencies. In the limit of $d \rightarrow \infty$ the Drude part can be expressed in terms of the quasi-particle weight, $\omega_p^{*2}/4\pi = (2e^2/3\hbar^2 a)DZ$. The ratio of the incoherent to the Drude contribution to the optical spectra in the paramagnetic phase can then be

Metal-Insulator Transitions Revisited

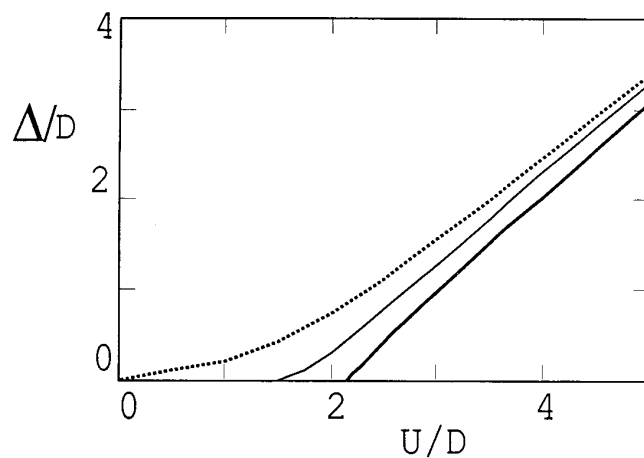


Figure 13 The gap in an unfrustrated antiferromagnetic phase, and in the paramagnetic (dotted line) phase, as functions of the interaction U .

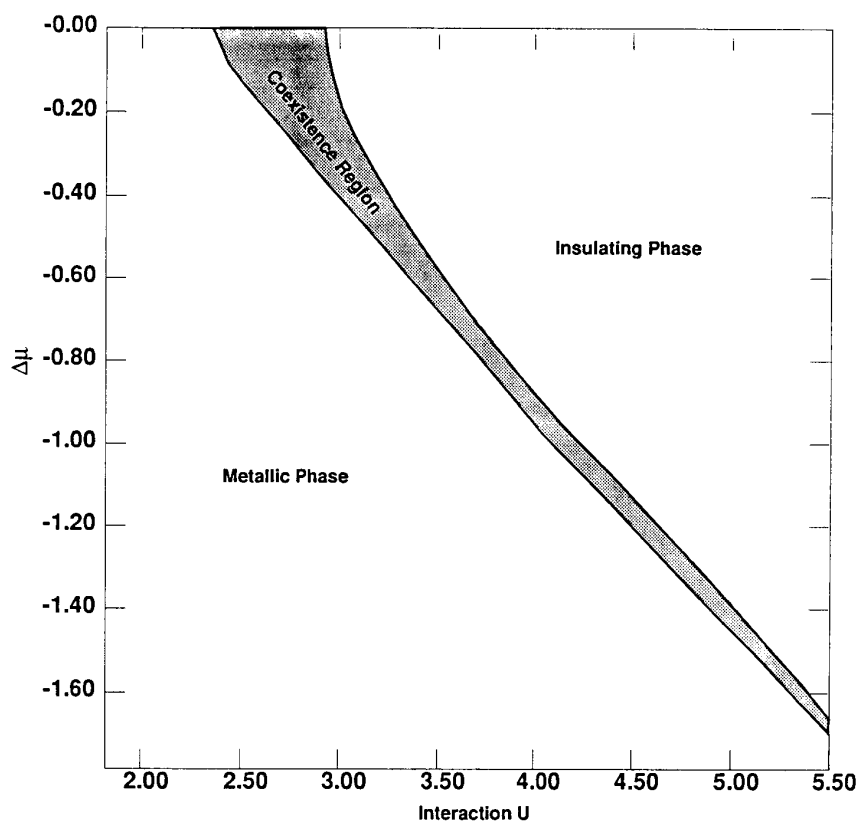


Figure 14 Phase diagram in the μ - T plane of the Hubbard model on a fully frustrated lattice at zero temperature.

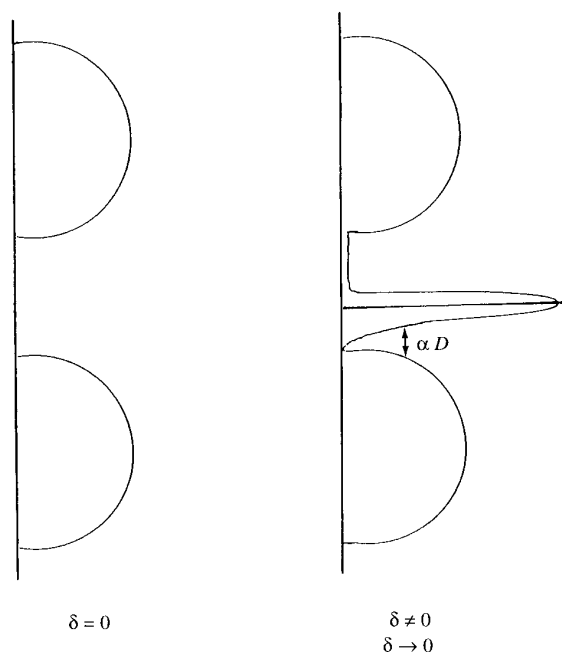


Figure 15 Evolution of the spectral function as one dopes *infinitesimally* the Mott insulator in the limit of large lattice coordination.

obtained from the kinetic energy, which is plotted as a function of U/D and shown in Fig. 12, and the quasi-particle residue. For comparison we also display the kinetic energy in the ordered phases in the same figure (from ref. 58).

We now turn to the gap of the insulating solution which was sketched in Fig. 9a.¹⁶ Unfortunately the determination of this quantity is subject to large numerical errors. In Fig. 13 (from refs 12, 58) an estimate of the gap is plotted as a function of U for the paramagnetic insulating solution, the unfrustrated and the partially frustrated antiferromagnetic solutions. As a definition for the magnitude of the gap we take twice the energy of the lowest-energy pole of the Green function obtained from the exact diagonalization method. It is clear, however, that as U is reduced, the gap of the paramagnetic insulating solution decreases. This is reminiscent of the Hubbard scenario. Notice that the gap of the partially frustrated model is smaller than the Slater gap and bigger than the gap of the paramagnetic insulating solution.

6 The Mott Transition as a Function of Doping

The mean-field technique has also been used to investigate the Mott transition as a function of doping in the Hubbard model. For non-integer *average occupancy* and in the paramagnetic phase there is only one solution of the mean-field equations. As a function of chemical potential, however, there is a region of coexistence of two solutions which describe a doped metal and an (asymmetric) insulator. The phase

Metal-Insulator Transitions Revisited

diagram in the $\mu-U$ plane of the Hubbard model on a fully frustrated lattice at zero temperature is shown in Fig. 14. It was obtained with the exact diagonalization method for $U = 4$.⁴⁸ The metallic solution is, also in this case, lowest in energy. The schematic evolution of the spectral function as one dopes the Mott insulator is shown in Fig. 15.^{20,21} It supports the basic ideas of the non-rigid (slave boson) picture. New states are created in a doped system that have no simple relation to those that existed in the insulator. A qualitative difference with respect to the slave boson results sketched in Fig. 4 is the fact that upon doping the resonance inside the Mott-Hubbard gap is well separated from the Hubbard band edges in the insulator.²⁰ This can be understood using the Luttinger theorem and the continuity of the mean-field solution describing the metallic state. The Hubbard model at half filling at U_{c2} has a well-formed, large, Mott-Hubbard gap. Near this value of U , the doped Mott insulator has states very near the middle of the gap. As U is increased the position of the resonance, or hole doping, moves toward the top of the lower Hubbard band. This is shown in Fig. 16. At infinite value of the interaction U , the resonance remains at a finite distance (of the order of a small fraction of the bandwidth) from the top of the Hubbard band.

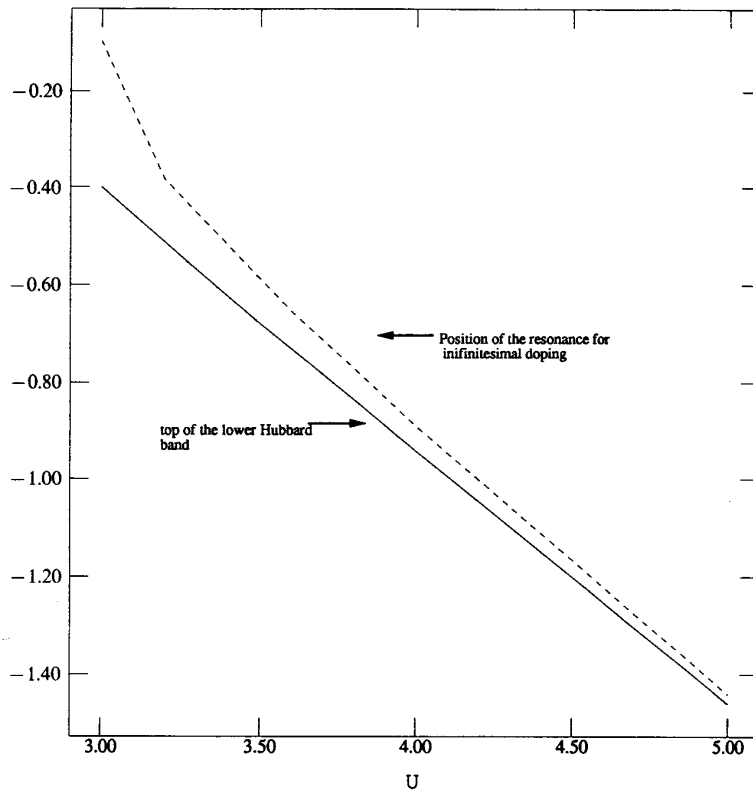


Figure 16 Position of the quasi-particle resonance for infinitesimal hole doping as a function of the interaction U (dashed line). The solid line indicates the top of the lower Hubbard band picture. Both are measured with reference to the half-full value of the chemical potential $U/2$.

Notice, however, that once the doping, $\delta \approx 1 - n$, becomes larger than a few per cent the resonance moves quickly inside the band and the qualitative results are very similar to those obtained with the slave boson method. From the point of view of the Anderson impurity model, there is a very fast crossover from the local moment regime to the mixed valence regime as the doping is increased. In Fig. 17 (from ref. 48) we show the evolution of the spectral function of the Hubbard model in infinite dimensions on a fully frustrated lattice. It was obtained with the exact diagonalization method, for $U = 4$. The spikes in the density of states in Fig. 17 are the result of the finite number of poles inherent to a diagonalization of a small system, but the position of the resonance is clearly seen, and it has merged with the continuum.

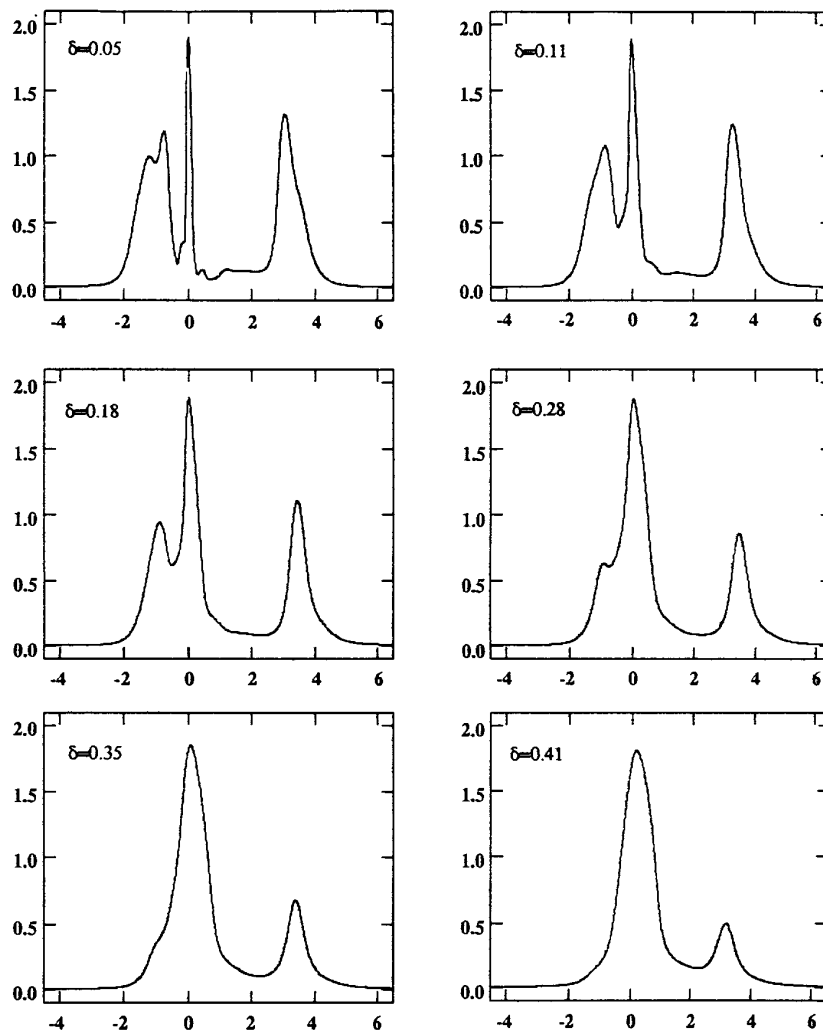


Figure 17 Evolution of the spectral function for finite doping the Mott insulator with $U = 4$.

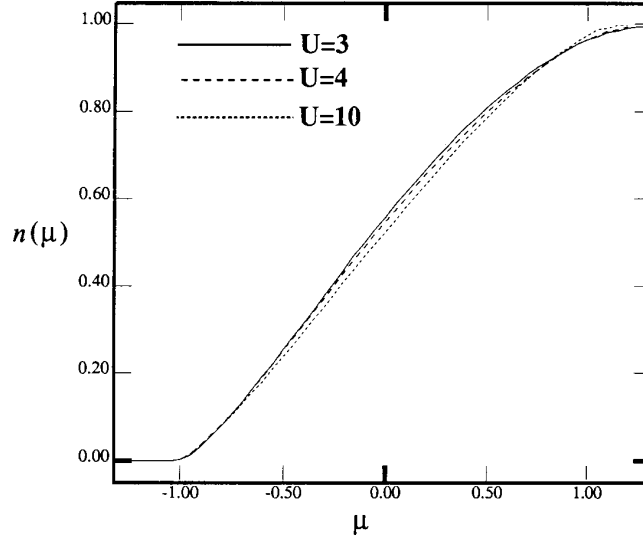


Figure 18 Particle number versus the chemical potential for different values of the interaction U .

The behavior of various physical quantities as a function of chemical potential and filling factor has been investigated. To convert doping to density we show the density as a function of chemical potential in Fig. 18. We note that the slope of the curve, i.e. the compressibility, goes to zero at $\mu = 0$ as U_c is approached. For bigger values of U , we have a vanishing compressibility characteristic of an insulating state. Notice that for $U > U_c$ the derivative of the density as a function of chemical potential approaches the zero doping, $\delta = 0$, limit with a finite slope. This is different than what has been observed in two dimensions.⁴⁹

To analyse the low-energy, low-temperature thermodynamics, one has to investigate the properties of the states which form the low-energy resonance. The Mott transition as a function of doping is also driven by the collapse of an energy scale, the vanishing of the weight in the Kondo resonance of the local picture, or equivalently the vanishing of the quasi-particle residue as the doping approaches zero for values of U above the Mott transition. If we denote by w the total weight in the low-energy resonance, $w \approx \delta a(U)$ for $U > U_{c2}$. When U is infinite a is equal to 0.5 and it increases rapidly as U is reduced. In infinite dimensions the vanishing of Z implies the divergence of the effective mass.

The specific heat and the magnetic susceptibility for $U = 3$ were calculated in ref. 16 using QMC at $\beta = 32$ in order to compare the theory with the experiments of Tokura *et al.*⁵⁰ on $\text{La}_x\text{Sr}_{1-x}\text{TiO}_3$. The specific heat is consistent with the parametrization $\gamma \sim 0.28\delta^{-1}$, and is expressed in units of $(\pi^2 k_B^2/3)\rho^0$, with $\rho^0 = 4/\pi D$. The spin susceptibility is expressed in units of μ_B^2/D and displayed together with the results of ref. 50 in Fig. 19 (from refs 16, 18).

The Wilson ratio $(\chi_s/\gamma)/(\chi_s^0/\gamma^0)$ as a function of doping is derived from these quantities and displayed in Fig. 20 (from ref. 18). Notice that it is approximately constant and its value is slightly lower than the experimentally observed value $R = 2$.

The total optical spectral weight of $\sigma(\omega)$ is given by $-(\pi/4)\langle T \rangle$, in units where e , a , $\hbar = 1$. In Fig. 21 (from refs 18, 48) we plot the kinetic energy $\langle T \rangle$ as a function

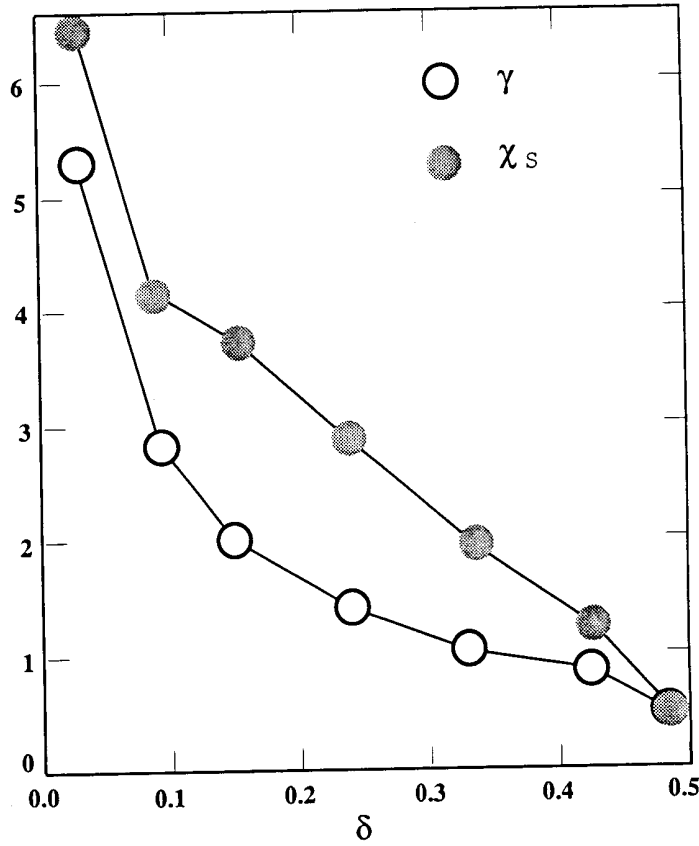


Figure 19 Specific heat and spin susceptibility as functions of doping for $U = 3$.

of the doping obtained from QMC at low temperatures and exact diagonalization. It is finite, of the order of the magnetic exchange at half filling, and it increases as one dopes the Mott insulator.

In infinite dimensions it is possible to make some rigorous statements about the behavior of the Hall coefficient approaching zero temperature. Since the current vertex can be neglected in the limit of vanishing wave number, the Hall coefficient can be evaluated directly in terms of the exact one-particle Green function. Since the self-energy only depends on frequency, the lifetime is wavevector independent and following the standard manipulations⁴⁶ which simplify in this case we obtain

$$R_H = \frac{-1}{ce} \frac{\sum_k \delta(\epsilon_k - \mu) [v_x^2 (\partial v_y / \partial k_y) - v_x v_y (\partial v_x / \partial k_y)]}{[\sum_k \delta(\epsilon_k - \mu) v_x^2]^2}. \quad (24)$$

It is remarkable that the Hall coefficient is given by the bare band structure even when the correlations are very strong. Notice, however, that at sufficiently high temperatures, the Kondo resonance is not present; the rigid Hubbard picture is then reliable and the Hall number is then expected to change sign. Monte Carlo simulations indicate that the Hall coefficient of the Hubbard model away from half filling is hole like,⁴⁷ a fact that can be understood if the simulations were performed at sufficiently high temperature.

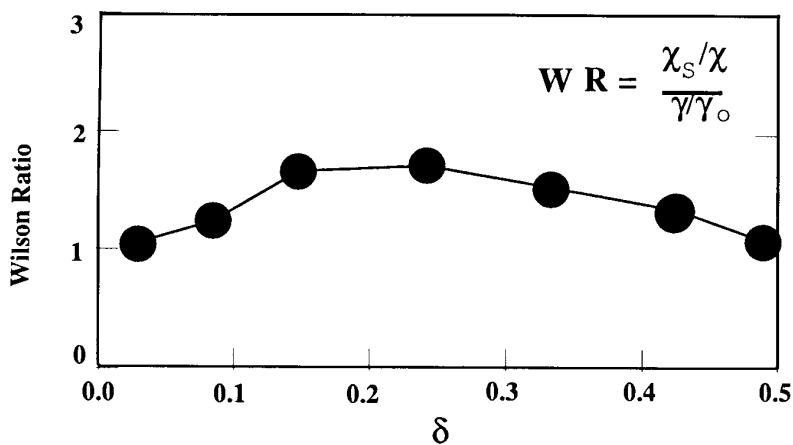


Figure 20 The Wilson ratio as a function of doping for $U = 3$.

7 Conclusions

We conclude with a comparison of some qualitative aspects of the experiments against the mean-field theory. In the last few years there has been significant progress in the experimental investigation of the Mott phenomena in transition-

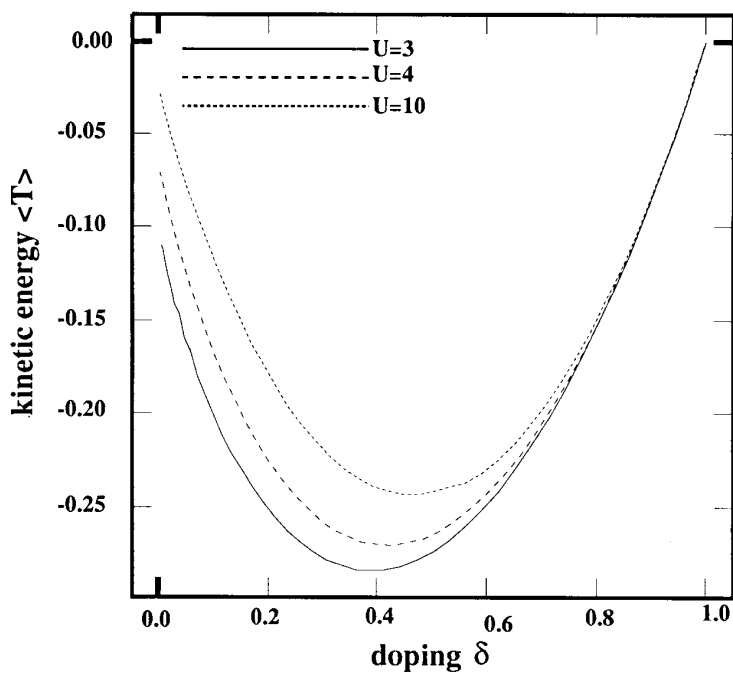


Figure 21 The kinetic energy as a function of doping for different values of U .

metal-based compounds. In the ternary compounds $\text{La}_{1-x}\text{Sr}_x\text{TiO}_3$ and $\text{Y}_{1-x}\text{Ca}_x\text{TiO}_3$ the Mott transition as a function of doping was realized by varying x .

The more traditional compounds, $\text{V}_{2-x}\text{O}_{3-\delta}\text{Cr}_x$ and $\text{NiS}_{2-x}\text{Se}_x$ which realize the Mott transition and the metal charge transfer insulator transition at half filling by varying x , have been investigated more thoroughly.³⁷ A similar study on the $\text{Ca}_{1-x}\text{Sr}_x\text{VO}_3$ system has also been reported.⁵²

In order to carry out a meaningful quantitative comparison of the predictions of the theory against the experimental results one has to incorporate the orbital degeneracy of the d^1 configuration in the theoretical treatment. While this work is still being carried out it is useful to point out that the comparison of the results of the one band model described above with the experimental data is very encouraging. The solution of the Hubbard model in the limit of large dimensions not only has provided a limit where various early ideas can be put in perspective, but seems to account for many puzzling features of the phase diagram and the photoemission spectroscopy of transition metal oxides.

The nature of the phase diagram of the Hubbard model and the issue of whether a metal-insulator transition can take place in the absence of magnetic order have been clarified. The phase diagram presented in Fig. 7 answers this question in the affirmative for a frustrated lattice. The phase diagram has the same topology as the experimentally observed phase diagram of V_2O_3 .⁴² There is a first-order boundary line where the two very different solutions cross in free energy, and several quantities experience a jump. The first-order line has a negative slope indicating that the paramagnetic insulating phase has a higher entropy than the metallic phase. The line ends in a second-order critical point; above it there is a smooth crossover between a metallic and an insulating regime. The slope of the crossover line at very high temperatures has a positive slope and is determined by the activation across the Mott-Hubbard gap. Even the small region of metallic antiferromagnetism which is predicted by the theory was found in recent neutron scattering experiments.⁵³

The corundum structure of V_2O_3 is not magnetically frustrated, but it becomes frustrated owing to the interplay with orbital ordering as suggested by Castellani *et al.*⁵⁶ Rice has recently revived this idea, showing that orbital ordering is consistent with recent neutron scattering experiments.⁵⁷ The relevance of a *frustrated* Hubbard model to V_2O_3 is now on a more solid footing.

The evolution of the spectral function as measured by photoemission spectra was followed by Fujimori⁵¹ in a series of compounds with one 3d electron per transition metal ion. In the series ReO_3 - VO_2 - LaVO_3 - LaTiO_3 - YTiO_3 the ratio of effective interaction U to the bandwidth D gradually increases. Fujimori observed that the Mott transition is driven by a transfer of spectral weight from low energy to high energy and that the Mott-Hubbard gap is well formed by the time that one reaches the Mott transition. This is in complete agreement with the scenario of ZRK. Notice, however, that in this compound the d electrons occupies a triply degenerate T_{2g} orbital and it is necessary to study how the effects of orbital degeneracy modify the ZRK scenario. This is particularly imperative since it is clear that the orbital degeneracy is responsible for the anomalously low Néel temperature of this compound. In an orbitally degenerate system, the insulator must be spin and orbitally ordered. The large degeneracy strongly suppresses the ordering temperature.

While Fujimori's experiments are consistent with the evolution of the metallic solution, recent optical studies of V_2O_3 are consistent with the evolution of the

insulating solution depicted in Fig. 9(a). In this case the insulating solution has to be thought of as the frustrated limit of the magnetic solution which is the ground state in the phase diagram of Fig. 7. In this scenario the metal–insulator transition is driven by the closure of the Mott–Hubbard gap. A comparison of the theoretical predictions for the integrated spectral weight and the optical gap as a function of U/D with the experimental observations has been carried out.^{54,58} The agreement is surprisingly good. Extracting U/D from the experiment we were led to predict an anomalous transfer of spectral weight as a function of temperature in the *metallic* phase of V_2O_3 . This seems to be in agreement with the experimental observations.⁵⁵

To account for the experiments in V_2O_3 and the evolution of the spectral weight observed in photoemission one has to use the two solutions, which should then cross at an intermediate value of U , in a partially frustrated situation. A more quantitative study on a more realistic lattice structure with orbital degeneracy is worth pursuing.

We have also calculated the behavior of various physical quantities as a function of doping and find a reasonable agreement with recent experiments of⁵⁰ in the $La_xSr_{1-x}TiO_3$ system provided that x is not very small. It is important to stress that both from the experimental and the theoretical point of view, it is not possible to approach the transition very closely. Theory and experiment agree fairly well down to dopings close to order 0.05. From the experimental point of view magnetic long-range order and the disorder caused by the random location of the dopants become important. From a theoretical point of view effects that are not properly taken into account by the mean-field theory become very important as the transition is approached. One of these effects is the magnetic exchange. In the mean-field theory magnetic correlations are ignored. We know from studies using the large- N expansion⁴⁴ that these effects are singular perturbations as the transition is approached.

With the same caveats as before concerning the role of orbital degeneracy the theory accounts for all the experimental observations by Tokura *et al.*:⁵⁰ (i) the transition as a function of doping is driven by the collapse of an energy scale, i.e. the specific heat effective mass diverges; (ii) the Wilson ratio is constant not too close to the transition; (iii) the low-temperature resistivity obeys $\rho = AT^2$ and A is proportional to γ^2 , and the A/γ^2 is large as in the heavy fermion systems; (iv) the Hall coefficient is electron like and essentially unrenormalized from the band structure value.

The mean-field theory, which becomes exact in the limit of large dimensionality, is a very powerful tool to unravel the physics of three-dimensional transition metal oxides. We have demonstrated that the analysis of the mean-field equations not only has allowed us to unify in a single framework some of the most relevant previous ideas on the metal–insulator transition, but more importantly it has provided new paradigms to model the evolution of the spectral weight as the Mott transition is approached.

The next step is to introduce more realistic density of states, crystal structures, and orbital degeneracies to achieve an *ab initio* description of the spectroscopies of correlated electron systems. The first step is a standard LDA calculation to obtain the band structure of the relevant compound. As a second step the LDA wave functions should be used to evaluate the Racah parameters which define the local on-site interactions between the relevant orbitals.⁵⁹ With this input one can proceed

to solve the mean-field equations with the relevant orbitals and interactions to obtain the local one-particle Green function and possibly other local response functions.

Another important direction is to go beyond the mean-field theory, to capture effects that are missed in infinite dimensions, and to assess the region where the mean-field treatment breaks down. Several approaches, such as a loop expansion,⁴¹ a different scaling of the interactions,⁶⁰ and an extension to larger clusters,⁶¹ have been suggested, but this area of research is at the present time largely unexplored.

Acknowledgments

I would like to thank my collaborators G. Moeller, M. Rozenberg, X. Y. Zhang, Vlad Dobrosavlevic, Antoine Georges, Daniel Fisher, Werner Krauth and Henrik Kajeuter for the interactions leading to the results described here.

This work has been supported by the National Science Foundation DMR 92-4000. Part of this manuscript was written while I visited the Hebrew University in Jerusalem. I acknowledge the Lady Davis Fellowship Trust for financial support and thank A. Schofield and V. Zevin for a critical reading of this manuscript.

References

1. MOTT, N. F., *Proc. R. Soc.* **A62**, 416 (1949).
2. MOTT, N. F., *Adv. Met. Phys.*, **3**, 76 (1952).
3. MOTT, N. F., *Can. J. Phys.*, **34**, 1356 (1956).
4. MOTT, N. F., *Philos. Mag.*, **6**, 287 (1961).
5. FINKELSHTEIN, A. M., *Z. Phys B* **56**, 189 (1984).
6. HUBBARD, J., *Proc. R. Soc.*, **A281**, 401 (1964).
7. METZNER, W. and VOLLHARDT, D., *Phys. Rev. Lett.*, **62**, 324 (1989).
8. GEORGES, A. and KOTLIAR, G., *Phys. Rev. B* **45**, 6479 (1992).
9. GEORGES, A., KOTLIAR, G. and SI, Q., Proceedings of the Trieste Meeting on Strongly Correlated Electron Systems. *Int. J. Mod. Phys. B* **6**, 705 (1992).
10. For recent reviews of these and related topics see: VOLLHARDT, D., in *Correlated Electron Systems V* Emery Editor World Scientific, Singapore and KOTLIAR, G. in *Strongly Correlated Electronic Materials*, ed. K. S. BEDELL, Z. WANG, D. MELTZER, A. BALATSKY, and E. ABRAHAMS, Addison-Wesley, Reading, MA (1994). For a comprehensive review see GEORGES, A., KOTLIAR, G., KRAUTH, W. and ROZENBERG, M. to appear in *Rev. Mod. Phys.*
11. JARRELL, M., *Phys. Rev. Lett.* **69**, 168 (1992).
12. ROZENBERG, M., ZHANG, X. Y. and KOTLIAR, G., *Phys. Rev. Lett.* **69**, 1236 (1992). ROZENBERG, M., *PhD thesis*, Rutgers University.
13. GEORGES, A. and KRAUTH, W., *Phys. Rev. Lett.*, **69**, 1240 (1992).
14. ZHANG, X. Y., ROZENBERG, M. J. and KOTLIAR, G., *Phys. Rev. Lett.*, **70**, 1666 (1993).
15. GEORGES, A. and KRAUTH, W., *Phys. Rev. B* **48**, 7167 (1993).
16. ROZENBERG, M. J., KOTLIAR, G. and ZHANG, X. Y., *Phys. Rev. B* **49**, 10 181 (1994).
17. ROZENBERG, M. J., MOELLER, G. and KOTLIAR, G., *Mod. Phys. Lett. B* **535**, (1994).
18. KOTLIAR, G. and ROZENBERG, M., To appear in the Proceedings of the Conference on the Mathematics and Physics of the Hubbard Model, San Sebastian (1994).
19. MOELLER, G., SI, Q., KOTLIAR, G., ROZENBERG, M. and FISHER, D., *Phys. Rev. Lett.*, **74**, 2082 (1995).
20. FISHER, D., KOTLIAR, G. and MOELLER, G., to be published.
21. KAJUETER, H., KOTLIAR, G. and MOELLER, G., to be published.
22. BRINKMAN W. F. and RICE, T. M., *Phys. Rev. B* **2**, 4302 (1970).

Metal-Insulator Transitions Revisited

23. GUTZWILLER, M., *Phys. Rev. Lett.* **10**, 159 (1963).
24. ESKES, H., MEINDERS, M. B. J. and SAWATZKY, G. A., *Phys. Rev. Lett.*, **67**, 1035 (1991).
ESKES, H. and SAWATZKY, G. A., *Phys. Rev. B* **43**, 119 (1991).
25. KOTLIAR, G. and RUCKENSTEIN, A., *Phys. Rev. Lett.*, **57**, 1362 (1986).
26. CASTELLANI, C., KOTLIAR, G., GRILLI, M., WANG, Z. and ROZENBERG, M., *Phys. Rev. Lett.*, **69**, 2009 (1992). BANG, Y., CASTELLANI, C., GRILLI, M., KOTLIAR, G., RAIMONDI, R. and WANG, Z., *Int. J. Mod. Phys. B* **6**, 531 (1992). RAIMONDI, R. and CASTELLANI, C., *Phys. Rev. B* **48**, (1993) 11453.
27. SLATER, J. C., *Phys. Rev.* **82**, 538 (1951).
28. MULLER-HARTMANN, E., *Z. Phys. B* **74**, 50. (1989).
29. BRANDT, U. and MIELSCH, C., *Z. Phys. B* **75**, 365 (1989).
30. JANIS, V., *Z. Phys. B* **83**, 227 (1991).
31. JANIS, V. and VOLLHARDT, D., *Int. J. Mod. Phys. B* **6**, 731 (1992).
32. CAFFAREL, M. and KRAUTH, W., *Phys. Rev. Lett.*, **72**, 1545 (1994). SI, Q., ROZENBERG, M., KOTLIAR, G. and RUCKENSTEIN, A., *Phys. Rev. Lett.*, **72**, 2761 (1994).
33. PRUSCHKE, TH., COX, D. L. and JARRELL, M., *Europhys. Lett.*, **21**, 5 (1993), and *Phys. Rev. B* **48**, (1993).
34. CYROT, M., *J. Phys. Paris* **33**, 125 (1972).
35. MORIYA, T. and HASEGAWA, H., *J. Phys. Soc. Jpn* **48** 1490 (1980).
36. CASTELLANI, C. *et al.* *Phys. Rev. Lett.* **43**, 1957 (1979).
37. SPALEK, J., DATTA, A. and HONIG, J., *Phys. Rev. Lett.* **54**, 728 (1987).
38. DAGOTTO, E., *Rev. Mod. Phys.* **66**, 763 (1994).
39. MOTT, N. F., *Metal-Insulator Transitions*, Taylor & Francis, London (1990).
40. MCWHAN, D. B., MENTH, A., REMEIK, J. P., BRINKMAN, W. F. and RICE, T. M., *Phys. Rev. B* **7**, 1920 (1973).
41. DOBROSAVLEVIC V. and KOTLIAR, G., *Phys. Rev. B* **50**, 1430 (1994).
42. KUWAMOTO, H., HONIG, J. M. and APPEL, J. *Phys. Rev. B* **22**, 2626 (1980).
43. WEGNER, F. *Z. Phys. B* **35**, 207 (1979).
44. GRILLI, M. and KOTLIAR, G. *Phys. Rev. Lett.* **64**, 1170 (1990).
45. MIYAKE, K., MATSUURA, T. and VARMA, C. M. *Solid State Commun.*, **71**, 1149 (1989).
46. FUKUYAMA, H. *Prog. Theor. Phys.* **42**, 1284 (1969). H. KOHNO, and K. YAMADA, *Prog. Theor. Phys.* **80**, 621 (1988).
47. JARRELL, M. and PRUSCHKE, T., *Phys. Rev. B* **49**, 1458 (1993) and *Z. Phys. B* **90**, **187** (1993). PRUSCHKE, T., COX, D. L. and JARRELL, M. *Phys. Rev. B* **47**, 3553 (1993).
48. KAJUETER, H., KOTLIAR, G. and MOELLER, G. preprint. MOELLER, G. *PhD thesis*, Rutgers University.
49. IMADA, M. *J. Phys. Soc. Jpn* **62** (1993) 1105. FURUKAWA, N. and IMADA, M. *J. Phys. Soc. Jpn* **60**, 3604 (1991).
50. TOKURA, Y., TAGUCHI, Y., OKADA, Y., FUJISHIMA, Y., ARIMA, T., KUMAGAI, K. and IYE, Y. *Phys. Rev. Lett.* **70**, 2126 (1993).
51. FUJIMORI, A. *Phys. Rev. Lett.* **69**, 1796 (1992).
52. FUJIMORI, A. *et al.* *Phys. Rev. Lett.* **74**, 2539 (1995).
53. CARTER, S. A., ROSENBAUM, T. F., HONIG, J. M. and SPALEK, J. *Phys. Rev. Lett.* **67**, 3440 (1992).
54. THOMAS, G. *et al.* *Phys. Rev. Lett* **73**, 11 (1994).
55. THOMAS, G. Private communication.
56. CASTELLANI, C., NATOLI, C. R. and RANNINGER, J. *Phys. Rev. B* **18**, 5001 (1978).
57. RICE, T. M. Private communication.
58. ROZENBERG, M., KOTLIAR, G. and KAJUETER, H. *et al.* *Phys. Rev. Lett.* **75**, 105 (1995).
59. ANISIMOV, V. and GUNNARSSON, O. *Phys. Rev. B* **43**, 7570 (1991).
60. KAJUETER, H. and KOTLIAR, G. Unpublished.
61. GEORGES, A. and KOTLIAR, G. Unpublished.